

# Mono-amino acid linkers enable highly potent small molecule-drug conjugates by conditional release

Yan Zheng,<sup>1</sup> Ruolin Xu,<sup>1</sup> Hong Cheng,<sup>1</sup> and Wanyi Tai<sup>1</sup>

<sup>1</sup>Department of Pharmacy, Zhongnan Hospital of Wuhan University, School of Pharmaceutical Sciences, Wuhan University, Wuhan, Hubei 430071, China

**The endosome cleavable linkers have been widely employed by antibody-drug conjugates and small molecule-drug conjugates (SMDCs) to control the accurate release of payloads. An effective linker should provide stability in systemic circulation but efficient payload release at its targeted tumor sites. This conflicting requirement always leads to linker design with increasing structural complexity. Balance of the effectiveness and structural complexity presents a linker design challenge. Here, we explored the possibility of mono-amino acid as so far the simplest cleavable linker (X-linker) for SMDC-based auristatin delivery. Within a diverse set of X-linkers, the SMDCs differed widely in bioactivity, with one (Asn-linker) having significantly improved potency (IC<sub>50</sub> = 0.1 nM) and fast response to endosomal cathepsin B cleavage. Notably, this SMDC, once grafted with effector protein fragment crystallizable (Fc), demonstrated a profound *in vivo* therapeutic effect in aspects of targetability, circulation half-life (t<sub>1/2</sub> = 73 h), stability, and anti-tumor efficacy. On the basis of these results, we believe that this mono-amino acid linker, together with the new SMDC-Fc scaffold, has significant potential in targeted delivery application.**

## INTRODUCTION

As famous targeted chemotherapeutic agents, antibody-drug conjugates (ADCs), have come into their own over the past decade. To date, the US Food and Drug Administration has approved 13 ADCs for clinical use in cancer therapy.<sup>1</sup> More than 100 ADCs are currently being evaluated in clinical trials.<sup>2,3</sup> The success of ADCs bolsters the concept of targeted chemotherapy and also provides a basis for developing other such agents for cancer treatment. In particular, small molecule-drug conjugates (SMDCs) are gaining growing attention.<sup>4–7</sup> Instead of utilizing monoclonal antibody (mAb) in ADCs, SMDCs carry toxic payloads to tumor cells by a small-molecule ligand. Its compact molecular size endows the SMDCs with numerous advantages such as deep penetration, low manufacturing cost, and good immune tolerance.<sup>4,8,9</sup> Moreover, its therapeutic effect can be further boosted by grafting with fragment crystallizable (Fc) or other effector proteins.<sup>10–12</sup> A number of SMDCs have been tested or are currently in clinical trials: vintafolide (EC145, a folate-vinblastine SMDC) completed a phase 3 trial but failed due to a lack of efficacy,<sup>13,14</sup> and Epopolate (BMS-

753493), PEN-886, and 4 other SMDCs of Endocyte's pipeline are in various stages of trials.<sup>15–18</sup>

Both ADCs and SMDCs are composed of an antigen-specific ligand (mAb or small molecule), a cytotoxic payload, and a chemical linker. All three components can markedly influence the therapeutic index, but the linker and its conjugation modality play critical roles in defining the degree of *in vivo* stability, the mechanism of action, and the profile of pharmacokinetics (PKs).<sup>19–21</sup> Furthermore, the overall *in vivo* performance of ADCs and SMDCs was largely dominated by these three key parameters.<sup>22</sup> The importance of linker design is reflected in the linkers' chemical commonality among 13 approved ADCs: 11 use the cleavable linker, and 7 of them use the dipeptide linker valine-citrulline-*p*-amino benzyloxycarbonyl (VCit-PABC) for payload delivery.<sup>23</sup> For cleavable linkers, the endocytic pathway of tumor cells can trigger the payload release in its free form, thus ensuring that the payload acts in its highest potency and also in favor of the so-called bystander killing effect.<sup>24,25</sup> While the non-cleavable linker acts in such a way that the payload is released together with the linker and the first amino acid residue of the conjugated antibody (in most cases, cysteine), resulting in the overall release of a bulky species payload-linker-Cys, which makes it less effective and less popular for application. Nevertheless, the protease-sensitive cleavable linkers, taking VCit-PABC as an example, contain relatively complex combinations, featuring a VCit dipeptide moiety and a self-immolative PABC spacer for conditional cleavage in endosomes.<sup>26–28</sup> This linker is not only enzyme-labile but also prone to cleave in acidic conditions, which is often troublesome during linker synthesis.<sup>29</sup> Moreover, it has been reported that the VCit-PABC linker can be partially hydrolyzed by certain plasma proteases, such as carboxylesterase 1C in rodent blood, leading to premature release of the toxic payload in circulation.<sup>30–32</sup> Significant effort has been directed toward balancing the stability of a cleavable linker in circulation and its lability for activation at the tumor site.<sup>33,34</sup>

Received 15 September 2023; accepted 15 February 2024;  
<https://doi.org/10.1016/j.ymthe.2024.02.020>

**Correspondence:** Wanyi Tai, Department of Pharmacy, Zhongnan Hospital of Wuhan University, School of Pharmaceutical Sciences, Wuhan University, Wuhan, Hubei 430071, China.

**E-mail:** [wanyi-tai@whu.edu.cn](mailto:wanyi-tai@whu.edu.cn)

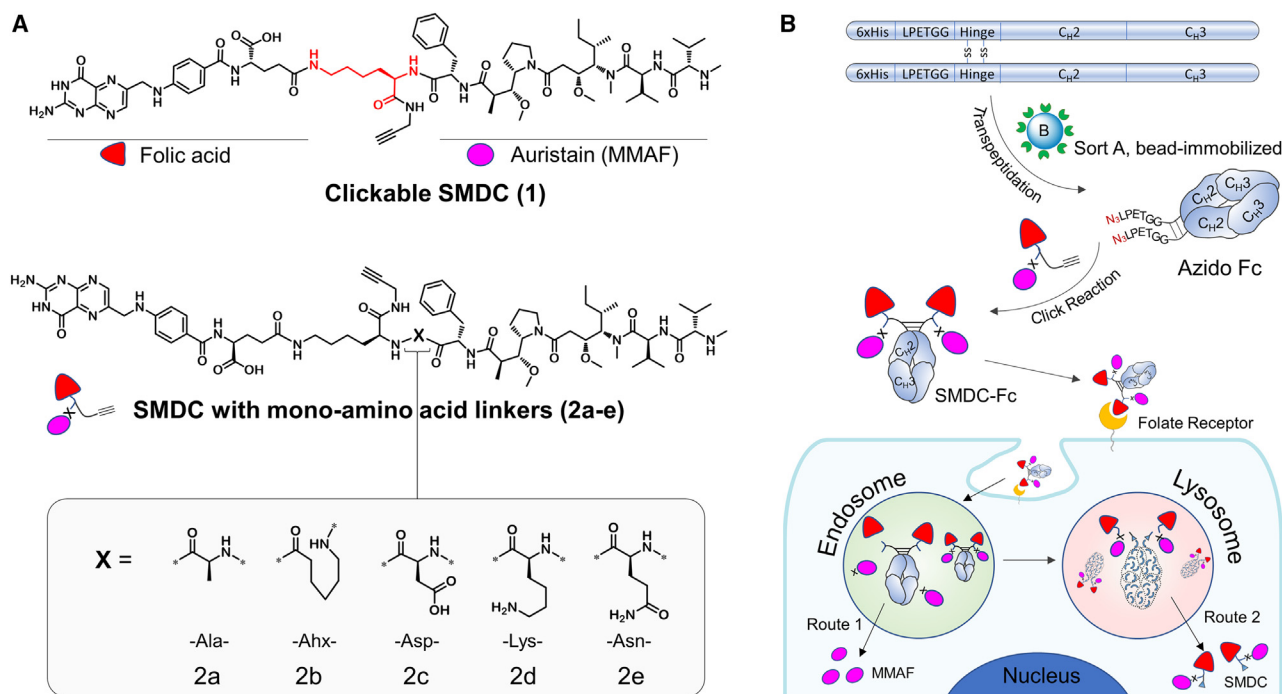


**Figure 1. Molecular structures of SMDCs and their corresponding delivery schematic**

(A) Structures of the clickable SMDC and its variants with mono-amino acid X-linkers. The SMDC was composed by a folate receptor (FR)-targeting ligand folic acid and the auristatin toxin MMAF. Between two components was inserted by a mono-amino acid (X-linker), such as Ala (2a), Ahx (2b), Asp (2c), Lys (2d), or Asn (2a), for controllable release. All SMDCs were installed with an alkyne handle for click reaction. (B) Schematic diagram of the Fc grafting and delivery strategy. Bacteria-expressed Fc protein was site-specifically modified with the azide group by bead-immobilized sortase A and then conjugated with SMDC to generate the long-circulating SMDC-Fc scaffold. After FR-mediated internalization, the scaffold was processed by endosomal protease to release the payload MMAF if the X-linker is cleavable (route 1) and was otherwise degraded by lysosomal proteolysis to free the SMDC for cytotoxicity (route 2).

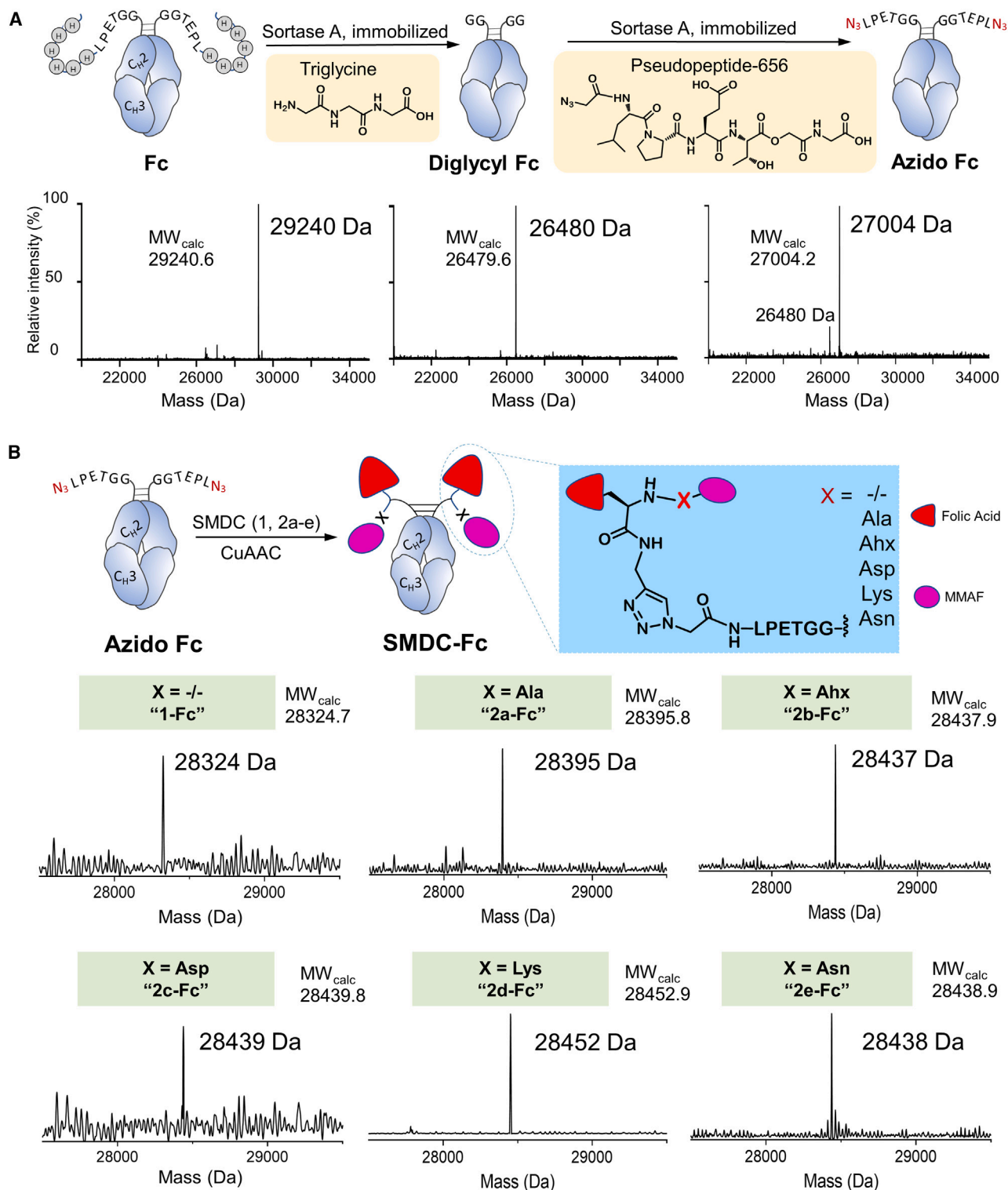
The non-cleavable linkers, on the other hand, are well characterized by their simple structure and high stability in circulation. As a rule, the simpler the better. Refining the aforementioned cleavable linker into a short pattern might be an option worthy of attention. Considering the broad substrate spectra of the acid-dependent proteases in endosome,<sup>35,36</sup> we envisioned that the simple mono-amino acid (mono-peptide) linkers might act as substrates as sensitive as dipeptide (VCit) or tetrapeptide (DS8201) linkers while keeping stable in circulation. In this article, we showed the development of an auristatin conjugate that incorporates a mono-amino acid linker (X-linker) for efficient endosomal cleavage and high therapeutic potency. After comparing a series of SMDCs bearing different X-linkers, an asparagine (Asn-linker)-containing SMDC was identified and chosen for further protein conjugation because of its high potency *in vitro* and its effectiveness in release. We demonstrated that the Fc protein-grafted auristatin conjugate (SMDC-Fc) using the Asn-linker exhibited extremely long blood circulation and profound anti-tumor efficacy in xenograft mice bearing small or large advanced KB tumors. Furthermore, we revealed that SMDC-Fc was mainly metabolized in the liver, which was distinct from the kidney tropism of the comparator SMDC. Our finding provides an applicable approach for designing cleavable linkers and developing new molecular classes for targeted chemotherapy.

## RESULTS

### Mono-amino acid linker design and SMDC synthesis

Auristatin analog MMAF (monomethyl auristatin F) was selected as the chemical toxin in this study (Figure 1A). This anti-mitotic toxin is the second most popular auristatin for antibody conjugation, just after its analog MMAE. Despite the commonality in potency and chemical structure, MMAF is well suited for derivatization with non-cleavable linkers since its anti-tumor potency can tolerate chemical modifications. Conversely, MMAE is only active in its native form. Another noteworthy aspect is that MMAF contains a C-terminal carboxylic acid group, which can be used as a point for conjugation. In this regard, we incorporated a mono-amino acid X-linker at the C terminus of MMAF and evaluated its impact on the therapeutic efficacy of SMDCs.

We first produced a non-cleavable auristatin conjugate (SMDC 1) by directly coupling the MMAF C terminus with folate receptor (FR)-targeting ligand folic acid without any X-linker. We expected that MMAF would keep most of its potency by virtue of its tolerance to derivatization. We then set out to assess a panel of mono-amino acid X-linkers appended to the C-terminal phenylalanine residue of MMAF. This subset of SMDCs consisted of the folate-X-MMAF unit, where X is alanine (2a), aminohexanic acid (2b), aspartic acid



(2c), lysine (2d), or asparagine (2e), respectively (Figure 1A). We expected that comparing the X-linker of interest with SMDC 1 would demonstrate the degree of improvement to the non-cleavable design. As our goal was to introduce a potential position that could be enzymatically cleaved inside endosomes of target cells, other potential hydrolysis sites in the structure of SMDCs should be blocked in order to increase the stringency of free drug release through X-linker proteolysis. The supporting-binding spacer (highlighted as red in Figure 1A) of folic acids, in SMDC 1 and 2a–2e, was reoriented to conjugate at the epsilon position of the lysine amine side to minimize the enzymatic hydrolysis, and the carboxylic side was amidated with propargylamine, as a chemical handle for click reaction with Fc proteins.

It was planned that all SMDCs would be grafted by Fc proteins to improve their biological performance *in vivo*. After receptor-mediated internalization, the toxin would be released from Fc in two proposed routes depending on the cleavability of the X-linker, as shown in Figure 1B. For most cleavable X-linkers, toxin release (shown as route 1) would be triggered early in the endocytic pathway. A short delivery algorithm enables MMAF release quickly in tumors and, more importantly, as its native form to elicit the highest potency and bystander effect. As for non-cleavable linkers, the delivery requires Fc proteolysis inside the lysosome to release the bioactive SMDC for tumor cell killing (route 2). After Fc catabolism, the released SMDC bears the hydrophilic folic acid and the first amino acid residue of the conjugated Fc protein, which likely results in an attenuated potency and limited membrane permeability. As this point indicates, SMDCs with cleavable X-linkers would be more bioactive than the non-cleavable ones, and the X-linker hydrolysis activity likely can modulate the conjugates' potency.

The synthesis of SMDCs proceeded through a three-step route involving folic acid synthesis, X-linker derivatization, and MMAF coupling. Previous synthesis of folate-drug conjugation involved a simple treatment of folic acid with the drug or linker in the presence of the condensing agent.<sup>37,38</sup> This practice often produced an inseparable mixture of  $\alpha$ - and  $\gamma$ -conjugates due to the presence of two carboxylic groups within the folate molecule. In order to selective conjugation of folic acid at the  $\gamma$  position, we first coupled the activated  $\gamma$ -carboxylate of glutamic acid 5 with the free amine of spacer 8, followed by furnishing with the pteric acid moiety, to produce the  $\gamma$ -conjugated folate-spacer 11 (Figure S1). The 2-(trimethylsilyl)ethyl (TMSE) and N<sup>10</sup>-trifluoroacetyl (Tfa) protecting groups are essential to the solubility of 11 in organic solvent. In particular of the Tfa group, after its concomitant deacylation in the Fmoc deprotection reaction (20% piperidine in DMF), product 12 turned to be almost insoluble in DMF. Nevertheless, the products afterward (13a–13e and 14a–14e) return to being soluble in common organic solvents, which makes the following reactions and purifications less

troublesome. Despite the absence of protection of the N<sup>10</sup>-amine group in compound 12, surprisingly, we did not observe noticeable side reactions during the coming X-linker derivatization and MMAF coupling reactions, likely due to the weak nucleophilicity of the phenyl nitrogen. Subsequently, the TMSE and Boc groups were cleaved under routine conditions, liberating the two termini and affording the SMDC in overall good yield. Due to the convergent nature of the synthetic process, it was possible for us to produce six SMDCs with variable mono-amino acid linkers simultaneously. As confirmed by high-resolution Orbitrap mass spectrometry (MS), the obtained SMDCs range from 1,300 to 1,500 Da in molecular weight (MW), which exceeds the threshold for membrane permeability (1,000 Da) but remains targetable to tumor cells by their folate ligands.

### Fc grafting and *in vitro* testing

The Fc domain is the key component of immunoglobulin G (IgG), which enables binding to the neonatal Fc receptor (FcRn) and recycles IgG for long circulation persistence. Fc protein grafting has been proven to be a broadly applicable strategy to improve the PKs of drugs. As shown in Figure 1A, SMDC 1 and 2a–2e have been structurally programmed with the alkyne chemical handle for copper-catalyzed alkyne-azide 1,3-dipolar cycloaddition (CuAAC) to Fc protein. To this end, we first need to engineer an azido Fc protein that bears an azide group to react with that alkyne handle. The His-tagged Fc protein was successfully expressed as a disulfide-linked homodimer in T7 shuffle bacteria and purified by rapid Ni-NTA affinity chromatography. To generate an Fc protein with the defined azide at the N termini, we first chop off the 6 $\times$ His tag together with the LPET motif by sortase A to produce a diglycyl Fc (Figure 2A). This product contains an N-terminal diglycine that can serve as a substrate of sortase A and can be transpeptidated by the azido-containing pseudopeptide-656 (synthesis shown in Figure S2), eventually yielding the desired azido Fc protein. As shown in Figure 2A, the electrospray ionization time-of-flight (ESI-TOF) mass analysis under reducing conditions confirmed the expected MW for Fc variants within each step of the construction process. The deconvolution result of azido Fc revealed two different peaks, which were assigned to the Fc variants diglycyl Fc (dwarf peak) and azido Fc (main peak), respectively. This observation described the imperfect turnover of the transpeptidation reaction, but its impact on the next step of grafting is negligible because integration of the mass peak areas leads to an overall purity > 90%.

To graft with Fc, SMDCs were incubated with the azido Fc protein in the presence of the stabilized Cu<sup>+</sup> species following a CuAAC protocol, as previously reported.<sup>39</sup> In our optimized miniature reaction, the SMDC-Fc conjugate can be synthesized at room temperature and cleaned up by a simple desalting step with an almost quantitative yield in a couple hours. This condition was confirmed by monitoring the click ligation reaction with SDS-PAGE (Figure S3). Only one

**methods.** The deconvoluted mass spectra of product in each step are showed on the bottom. The MW of Fc protein was calculated on a basis of post-translational modification with N-terminal methionine excision. (B) SMDC was grafted with azido Fc by CuAAC click chemistry. The deconvoluted mass spectra of SMDC-Fc products are depicted on the bottom. All the mass values present the MWs of the monomer chains because of the reducing condition during sampling.

A

Conjugates	Linker	[M-H] <sup>-</sup> Calcd	[M-H] <sup>-</sup> m/z	in vitro IC <sub>50</sub> (nM)		
				KB cell	HeLa	A549
1	-/-	1318.7318	1318.7224	9.34±2.78	57.25±33.05	> 1000
2a	Ala	1389.7689	1389.7632	3.60±1.27	17.92±8.38	> 1000
2b	Ahx	1431.8158	1431.8102	5.87±1.78	30.09±14.67	* > 1000
2c	Asp	1433.7587	1433.7532	3.04±1.09	20.31±10.01	* > 1000
2d	Lys	1446.8267	1446.8210	3.76±1.54	18.44±7.65	> 1000
2e	Asn	1432.7747	1432.7646	0.96±0.42	6.86±2.96	> 1000
1-Fc	-/-	28324.74	28324	1.84±1.36	36.83±18.90	> 1000
2a-Fc	Ala	28395.82	28395	1.48±0.78	10.51±3.75	> 1000
2b-Fc	Ahx	28437.90	28437	* 2.19±0.54	* 27.44±7.96	* > 1000
2c-Fc	Asp	28439.83	28439	* 1.37±0.67	* 11.35±4.30	> 1000
2d-Fc	Lys	28452.92	28452	1.72±1.02	12.06±4.47	> 1000
2e-Fc	Asn	28438.85	28438	0.10±0.02	2.07±0.74	> 1000

B

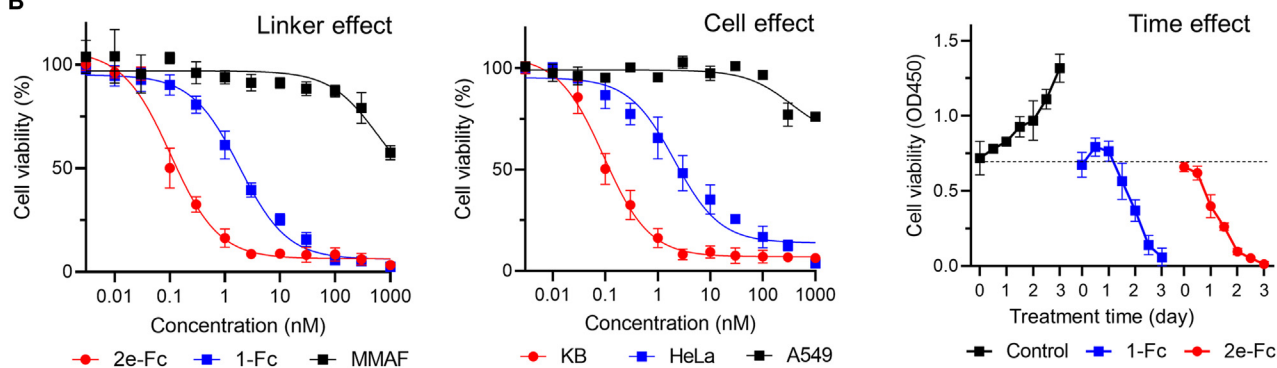


**Figure 3. In vitro potency of SMDC and SMDC-Fc to tumor cells**

(A) Characterization and IC<sub>50</sub> evaluation of auristatin conjugates on KB, HeLa, and A549 cells. Mass analysis of SMDC was performed on high-resolution Orbitrap mass spectrometry in negative ion mode. As for Fc-grafted SMDC, the deconvoluted data were provided. *In vitro* cytotoxicity was determined on human cancer cell lines with different FR expression levels, KB (+++), HeLa (++), and A549 (–). The IC<sub>50</sub> values were expressed as mean ± SD, \*\*p < 0.01. The dose-response curves are available in Figures S4 and S5. (B) Cytotoxicity profiles of SMDC-Fc. The best auristatin conjugate 2e-Fc (with cleavable Asn-linker) demonstrated much stronger cytotoxicity than the non-cleavable 1-Fc on KB cells (left). Its potency was also correlated to the FR expression level of tumor cells, suggestive of its selectivity and targetability (middle). 2e-Fc elicited its cytotoxicity effect much faster than 1-Fc due to the controllable release of payloads by the Asn-linker (right). The no-treatment group is referred to as control in this image.

slower-migrated band was observed after Fc grafting, indicating the predominance of the programmed product. This conclusion is in agreement with the result from the deconvoluted mass spectra of SMDC-Fc, in which all the conjugates' peaks shifted toward higher mass in comparison to azido Fc protein (Figure 2B). The concomitant increase in mass can perfectly match the MWs of the corresponding SMDCs, indicating the successful grafting of SMDC with Fc protein.

*In vitro* potency was tested firstly on FR-positive human oral epidermoid carcinoma KB cells *in vitro* using the non-cleavable auristatin conjugates 1 and 1-Fc as references. KB cells were incubated with serial dilutions of conjugates for 72 h, and cell viability was determined using

the standard Cell Counting Kit-8 (CCK-8) method (Figure 3A). Most conjugates with X-linkers elicited much higher potency than their references, indicating that the mono-amino acid linkers did follow the endosomal release route 1. One linker that emerged was amino acid Asn, which is a key residue of the proteolysis-resistant peptide linker poly-Asn and was assigned as a non-cleavable control in this study, but surprisingly, its auristatin conjugates 2e and 2e-Fc were both the most potent in their groups (IC<sub>50</sub> = 0.1 nM, 18 times lower than the non-cleavable counterpart). This trend was persistent when we tested them on HeLa cells. They remain the most potent, but their IC<sub>50</sub> values were slightly higher than that on KB cells, in agreement with the lower expression level of FR on HeLa cells. Apparently, another cell line,

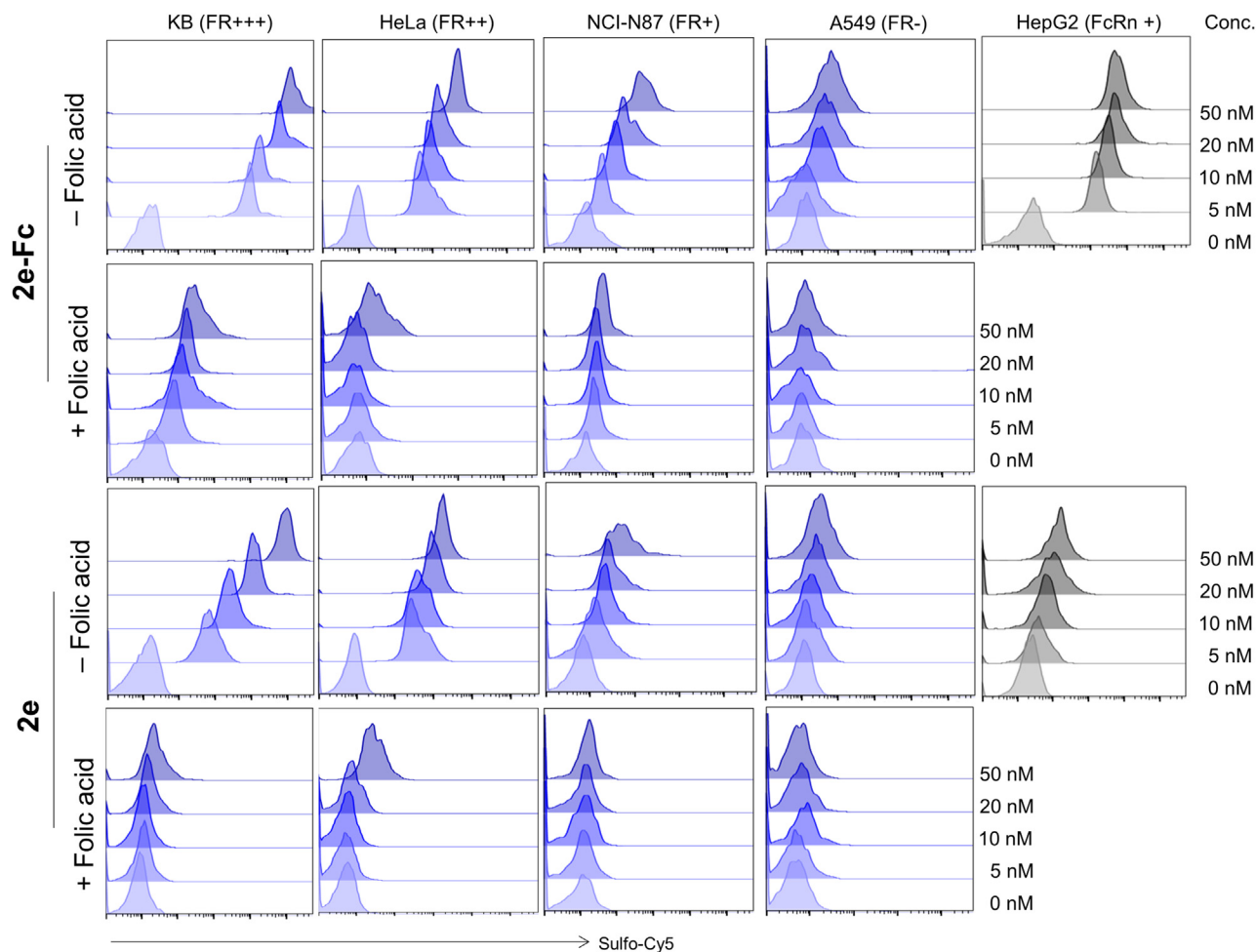


**Figure 4. The delivery of auristatin conjugates to tumor cells**

The avidity analysis of 2e and 2e-Fc to the FR or FcRn of tumor cells by fluorescence-activated cell sorting (FACS). The binding of the conjugates with KB cells (FR+++), HeLa cells (FR++), NCI-N87 (FR+), and A549 cells (FR-) was analyzed in the presence or absence of free folic acid (4  $\mu$ M). Results are shown as histogram overlay of serial concentrations of the conjugates within different cell populations. HepG2 cells expressing human FcRn were evaluated with serial dilutions of conjugates at pH 6.0 to confirm the functionality of the Fc domain.

A549, which does not express FR, was unaffected after drug treatment (Figure 3B). In parallel, we tittered the 3-day growth curve of KB cells treated by 1-Fc and 2e-Fc, respectively. The conjugate 1-Fc displayed an inverted J curve, indicating that cells can be killed but that the growth was unaffected at the beginning. The delay of the cytotoxicity might be imputed to the necessity of a time window for Fc proteolysis and concomitant drug release, as shown by route 2 in Figure 1B. With few exceptions, 2e-Fc, which contains an Asn-linker for endosomal cleavage, exhibited a much faster effect of cytotoxicity.

#### Targeted delivery and cathepsin B-controlled release of MMAF

The broad activity of 2e and 2e-Fc raised a concern about their specificity and selectivity toward tumor cells. To elucidate this, the drug was labeled with the fluorescent dye sulfo-Cy5, and the conjugates were incubated with four tumor cell lines, selected based on their FR status: KB (+++), HeLa (++) , NCI-N87 (+), and A549 (-) cells.

The flow cytometry results shown in Figure 4 revealed that the avidity of both 2e-Fc and 2e to tumor cells was well in correlation with the FR expression levels, and the binding profile was displayed in a dose-dependent manner. We also noticed that 2e-Fc always showed a higher binding capability than its counterpart, 2e. Moreover, this advantage can be abolished by co-incubation with abundant folic acid competitors. These results indicated that both bindings are highly specific but that the affinity of 2e-Fc to FR is slightly higher than that of 2e. The increment in affinity is likely ascribed to the bivalency effect of 2e-Fc because the homodimer state of Fc can guarantee two SMDCs grafted in parallel for receptor binding (Figure S3).

Apart from the positive role of the bivalent effect, the Fc protein also takes part in IgG recycling and long circulation persistence by binding with FcRns as well.<sup>40</sup> The FcRn is expressed mainly on the endothelial cells of small arterioles and capillaries in muscle and liver.<sup>41</sup> After the

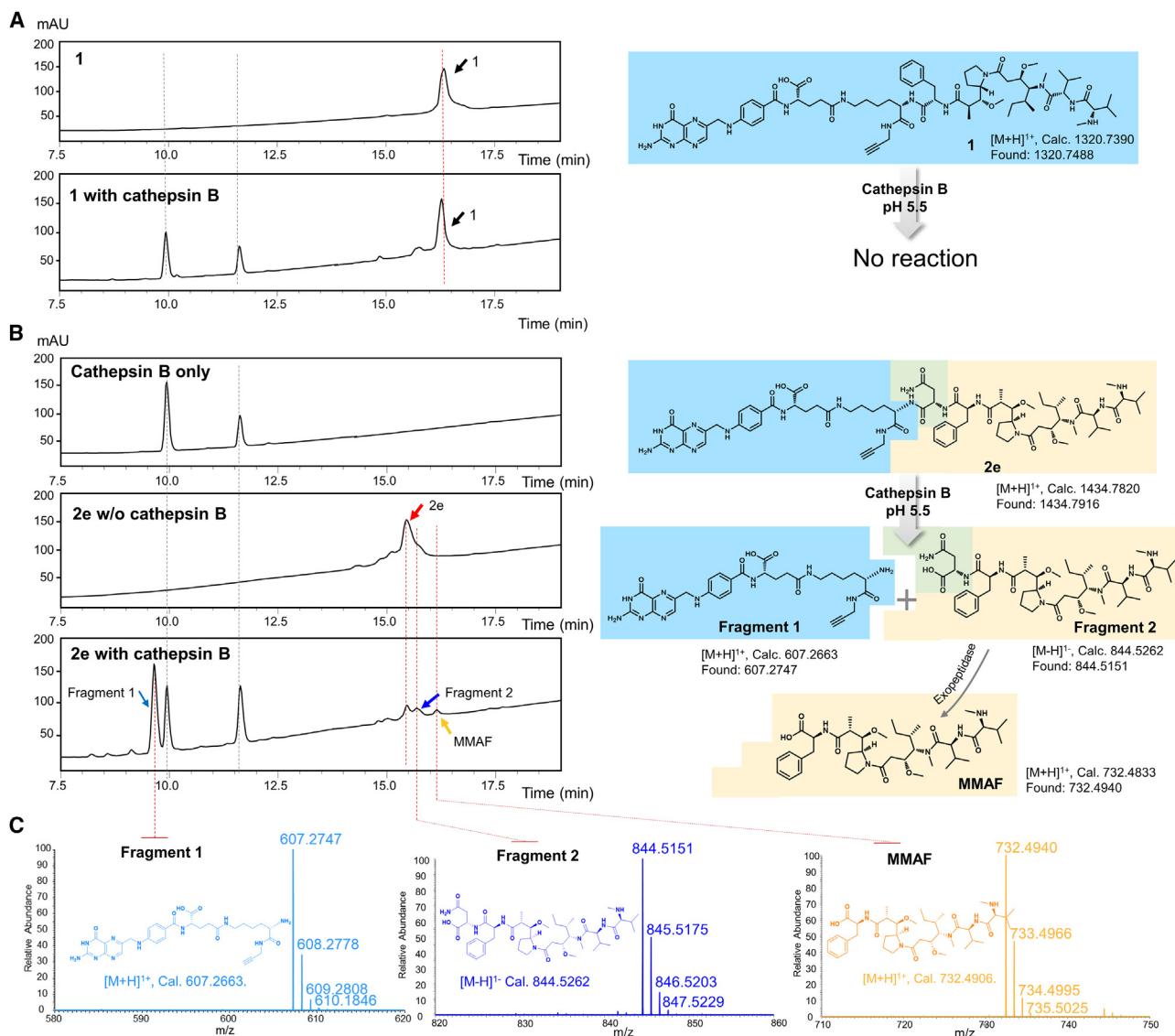


**Figure 5. Cathepsin B-mediated cleavage of SMDC at X-linker position**

(A and B) The activated cathepsin B was incubated at pH 5.5 with SMDC 1 and SMDC 2e, respectively. The HPLC spectra after proteolysis are listed on the left, and the interpreted routes of drug release are shown on the right. (C) The high-resolution mass spectra of fragments 1, 2, and MMAF were found after incubation of cathepsin B with SMDC 2e (Asn-linker). The MMAF release resulted from the loss of terminal Asn from the precursor (fragment 2) by exopeptidase.

fluid-phase pinocytosis, Fc binds FcRn at the acidic pH of endosomes, recycles with it to the plasma membrane, and finally can be released back into the circulation, resulting in a rescue of IgG from degradation. To investigate whether the SMDC-grafted Fc can be recycled, we incubated 2e-Fc with the FcRn-positive cell line HepG2 and confirmed that it can dose-dependently bind with the FcRn at the acidic pH. In contrast, SMDC 2e, which does not contain the Fc module, fails to be recognized by HepG2 cells (Figure 4).

Our interest in 2e-Fc was then aroused by its potential as a superpotent therapeutic agent. Besides the targetability aforementioned, the

mono-amino acid X-linker is a key factor accounting for the high potency of 2e-Fc in Figure 3. To investigate how the *in vitro* activity is modulated by a chemical modification to the X position, we evaluated SMDCs for cathepsin B-mediated cleavage. SMDC 1 and SMDC 2e were incubated in the presence of bovine spleen cathepsin B at pH 5.5. With few exemptions, high-performance liquid chromatography (HPLC) analysis confirmed that without an X-linker, SMDC 1 is quite stable in the presence of cathepsin B (Figure 5A). In contrast, SMDC 2e was consumed quickly in 1 h, and three nascent peaks emerged in the HPLC spectra (Figure 5B). The ESI-MS analysis revealed that the *m/z* values of these peaks were well correlated with the MWs of the

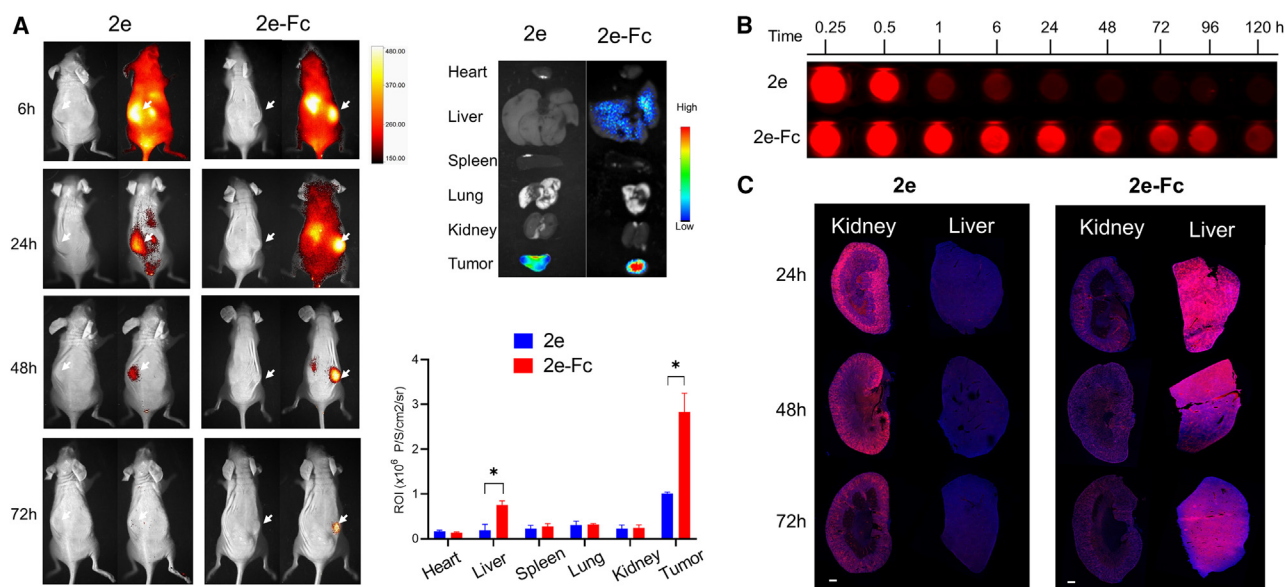


**Figure 6. Systemic biodistribution of auristatin conjugates in mice**

(A) *In vivo* tracking of conjugates 2e and 2e-Fc in mice bearing KB xenograft tumors. Whole-body biodistribution was monitored at indicated time points after tail vein injection of equivalent fluorescence units of conjugates (left). The dissected tumors and major organs were imaged after the experiments (72 h, top right) and quantified in three independent experiments (bottom right). Arrows indicate the tumor sites. \* $p < 0.05$ , data are shown as mean  $\pm$  SD. (B) Pharmacokinetics of conjugates 2e and 2e-Fc in mice blood after intravenous administration. The conjugates were labeled with the NIR dye sulfo-Cy7, and the red represents the fluorescent signal of the conjugates. (C) Kidney and liver distribution of 2e and 2e-Fc 24, 48, and 72 h after administration. The sulfo-Cy5-labeled conjugates are shown in red, and the nuclei stained with DAPI are shown in blue. Scar bar, 1 mm. Full images are available in Figures S7 and S8.

three fragments shown in Figure 5C. These results indicated that cathepsin B can recognize and cleave the amide bond between the Asn-linker and the supporting-binding spacer. The released fragment 2 (Asn-MMAF), as a form of prodrug, was further processed by exopeptidases to unfold the MMAF in its free form.

#### ***In vivo* efficacy studies**

With confirmation of SMDC-Fc efficacy *in vitro*, we set out to evaluate the potential of these auristatin conjugates to reach tumors *in vivo*. The conjugates 2e and 2e-Fc were labeled with the near-infrared (NIR) fluorescent dye sulfo-Cy7 and administered into the KB-tumor-bearing mice by tail vein injection. As shown in Figure 6A, the accumulation of both conjugates in tumors was observed 6 h after administration. However the tumor fluorescence of 2e began to decline and later became undetectable. By contrast, the tumors homed by the 2e-Fc remained visible even after 72 h. The observation was also confirmed by NIR imaging of the dissected organs and tumors, in which 2e-Fc can deposit almost 3 times more drugs at tumor sites than 2e (Figure 6A). The distribution disparity is likely ascribed to the Fc grafting strategy and the corresponding improvement in PKs. We then assessed the pharmacokinetic profile of 2e and 2e-Fc using BALB/c mice. After administration of equivalent doses of sulfo-Cy7-labeled conjugates, blood was collected periodically to analyze the drug retention in blood by an Odyssey infrared scanner. As shown in Figure 6B, persistent fluorescent signals were observed in the 2e-Fc group throughout all time points of the experiments, while

2e was completely clean from blood in less than 1 h. Quantitative analysis showed that the half-life of 2e-Fc in mice was 73 h, while SMDC 2e has a half-life of only 0.5 h (Figure S6).

The prolonged blood retention also has an impact on the conjugates' metabolic pathways. Histochemical analysis was undertaken to determine the drug deposition in two metabolic organs: liver and kidney. Mice were injected with sulfo-Cy5-labeled conjugates. At indicated time points, the organs were removed, and the frozen sections were evaluated for the presence of the conjugates using the Leica Aperio slide scanner. Figure 6C shows that 2e and 2e-Fc exhibited distinct deposition patterns in the two organs. 2e was exclusively detected in the kidney and barely seen in the liver, while more 2e-Fc was seen in the liver, with a significantly reduced kidney deposition. Both groups demonstrated a fluorescent signal decay with the extension of metabolic time, indicating the biodegradability of these conjugates.

We next extended the *in vivo* study to a set of anti-tumor treatment experiments for both conjugates with Asn-linkers. The KB xenograft model was selected for *in vivo* therapeutic evaluation. To explore the anti-tumor potential, two dosing regimens were scheduled for the treatment of small pre-established tumors and large advanced tumors, respectively (Figure 7A). The tumor growth curve in Figure 7B showed that a single dose (intravenous [i.v.], 5 mg/kg) of 2e-Fc demonstrated a robust cure to the small pre-established tumor

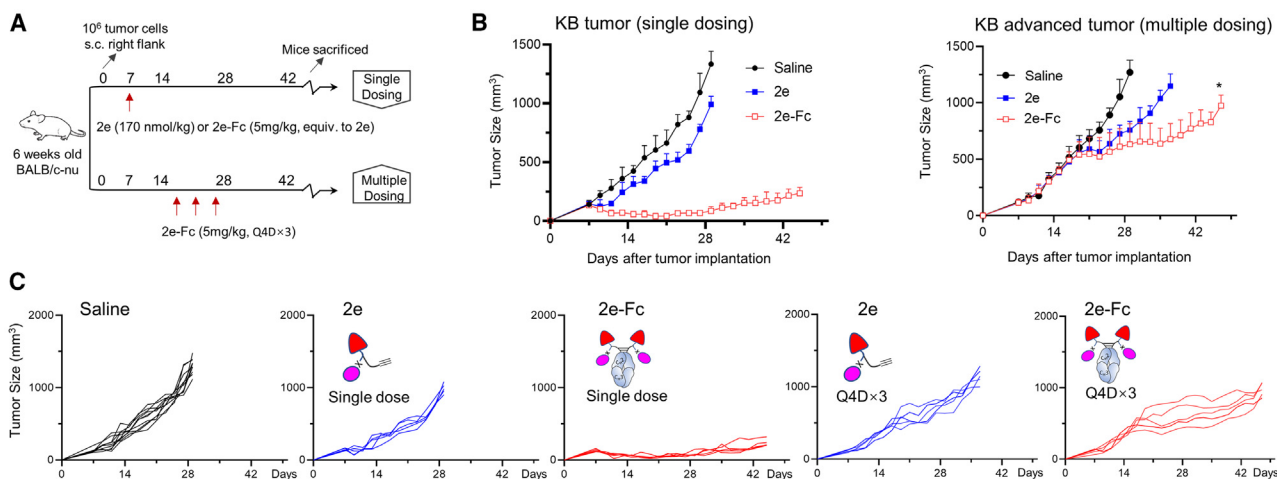


**Figure 7. Anti-tumor efficacy of auristatin conjugates 2e and 2e-Fc in KB xenograft mice**

(A) Dose regimens and timelines of the treatment. Q4Dx3: three doses, every 4th day. (B) Graph showing tumor volume changes after treatment. Mice bearing small pre-established KB tumors ( $100 \text{ mm}^3$ ) received only a single intravenous injection of 2e, 2e-Fc, or control saline (left). The exact doses of 2e-Fc (5 mg/kg) are equivalent to the 2e group at 170 nmol/kg conjugated MMAF per kg. As for advanced tumor treatment, the conjugates 2e-Fc (5 mg/kg) and 2e (170 nmol/kg) were injected on days 17, 21, and 25 after cell inoculation when the tumor volume reached about  $600 \text{ mm}^3$ . Mean tumor volumes ( $\text{mm}^3$ ) versus time (in days) after cell inoculation are plotted. \* $p < 0.05$ . (C) Individual tumor volume was graphed separately with  $n \geq 5$  mice per group ( $n = 10$  in the saline group and  $n = 5$  in all other groups).

xenografts (tumor burden  $\approx 100 \text{ mm}^3$ ). The therapeutic efficacy reached the late stage of experiments, indicative of the long-lasting and profound anti-tumor effect. By contrast, the anti-tumor effect of 2e was not as durable, and only a slight retardation of tumor growth was observed in the wake of drug administration (Figures 7B and 7C). This may be explained by the short half-life of 2e in blood circulation and the limiting tumor deposition of drugs within the single-dose regimen. In the advanced KB tumors (tumor burden  $\approx 600 \text{ mm}^3$ ), multiple injections (i.v., 5 mg/kg, Q4Dx3) of 2e-Fc led to tumor stabilization for up to 1 month, which was significantly longer than its counterpart, 2e (Figures 7B and 7C). Statistical tests revealed significant differences among the treatment groups ( $p < 0.05$ ). No toxicity was observed, as assessed by monitoring of clinical signs and body weight (Figure S9). Collectively, these data demonstrated that the auristatin conjugate with the Asn-linker was highly active in FR-positive xenograft models.

## DISCUSSION

We have investigated a class of mono-amino acid linkers that enable conditional release of auristatin drugs by cathepsin B for the first time. The amino acids in the linker library were chosen based on their susceptibility to proteases like other linkers sharing the same characteristics or sequences. Based on previous reports,<sup>19,42</sup> we expected that the Ala-linker would serve as a mimic of the Ala-Ala ADC linker with good cathepsin B sensitivity and mouse plasma stability. In parallel, we also devised the X-linker with aspartic acid and lysine, two highly polar residues that would enhance the water solubility of MMAF and increase its accessibility by cathepsin proteases. In particular, the Lys-linker in SMDC 2d was packed with the phenylalanine residue of MMAF to form a well-established Lys-Phe dipeptide, which was reported to be susceptible to cathepsin B cleavage.<sup>43</sup> The

Asn-linker (SMDC 2e) and the Ahx-linker (SMDC 2b) were exploited as controls, as poly-Asn and Ahx have been well known as stable linkers in engineered proteins.<sup>44,45</sup> The *in vitro* potency testing (Figure 3) revealed an expected trend Ala  $\approx$  Asp  $\approx$  Lys  $>$  Ahx  $>$  no linker, but surprisingly, the Asn-linker outperformed all other mono-amino acid linkers and demonstrated the highest potency. We also provided evidence of the fast cleavage of the Asn-linker by cathepsin B *in vitro*, confirming its conditional cleavability at the X-linker position. All the results indicated that amino acid derivatization of X-linkers can modulate the hydrolysis activity and thus may enable us to design more cleavable linkers in the future.

The clinical utility of SMDC relies heavily on the selectivity of this molecular module to FR. Flow cytometric data in Figure 4 demonstrated an FR-expression-level-dependent binding of SMDC to different cell types. This receptor selectivity was correlated well with the  $\text{IC}_{50}$  profiling results on three cell lines (Figure 3B). To further confirm the fidelity, we generated an FR-positive cell line by CRISPR-Cas9-mediated knockin of the FOLR1 gene (GenBank: NM\_000802.3) in HEK293 cells. This stable cell line HEK293/FR expressed a much higher level of FR than its parent cell line HEK293, as confirmed by western blotting analysis in Figure S10. The discrimination between  $\text{IC}_{50}$  curves of two cell lines demonstrated that FR overexpression did increase the cell susceptibility to the SMDC treatment (Figure S11), suggestive of the SMDC selectivity.

The use of the X-linker could serve as a simple but effective solution for the conditional release of MMAF from SMDC-Fc conjugates. The Asn-linker was preferentially chosen over other mono-amino acid linkers due to its fast response to cathepsin B treatment (Figure S12A). Its superiority was consistent with what we observed in the test for

*in vitro* cytotoxicity (Figure 3A). The Fc grafting has little impact on the linker accessibility by the cathepsin B, as the released MMAF metabolites were detected by LC-MS when we incubated 2e-Fc with cathepsin B (Figure S12B). It is worth noting that cathepsin B might be not indispensable for Asn-linker cleavage in the endosome, and other cathepsins or proteases may take part in the linker cleavage as well. For example, it has been reported that the Asn-containing tripeptides and dipeptide linkers are susceptible to the legumain, an asparaginyl endopeptidase that exhibits optimal activity at low pH in the endosome.<sup>35,46</sup> The cleavability of the Asn-linker by those endosomal proteases would promote the route 1 delivery algorithm, which is shorter in route and quicker in action. However, this route hypothesis needs to be further proven by monitoring the MMAF metabolites in cells or tumor tissues by a very sensitive analytical technique—i.e., the radiolabeled isotope technique or LC-tandem MS method.<sup>47–49</sup> It is of our interest to investigate the linker-dependent intracellular processing on SMDC-Fc in the future.

The prolonged blood circulation of 2e-Fc stems from the intrinsic function of Fc protein. It not only supports the SMDC-Fc recycling through its interaction with the FcRn but also prevents (at least slows down) the renal clearance due to the bulky size of the protein. It is well known that the typical kidney filtration threshold for proteins is around 50 kDa.<sup>50</sup> The small-molecule-based SMDC 2e (MW: 1.4 kDa; Figure S13) is generally renal clearable and can be rapidly eliminated from the body through the urinary system, reflected by a short serum half-life and high accumulation in the kidney (Figure 6). In contrast, 2e-Fc (MW: 57 kDa), due to the threshold effect, was prevented from renal elimination and thereby extended its half-life in the systemic circulation. Nevertheless, the long retention in the blood stream increased the deposition of 2e-Fc in the liver owing to the liver's large visceral mass and passive hepatic congestion. It is known that FcRn is also significantly expressed in hepatic cell populations including Kupffer cells and liver sinusoidal endothelial cells, which can help direct IgG or SMDC-Fc back toward the circulation instead of to the bile for clearance.<sup>51</sup> Meanwhile, whether the metabolism and clearance of 2e-Fc in the liver also rely on FcRn expression is unknown.

In our system, the linker-optimized SMDC was grafted with the effector protein Fc for better *in vivo* performance. Fc protein is of great therapeutic interest not only because it confers a long circulation half-life on its cargo by virtue of its favorable pH-dependent binding to FcRn<sup>52,53</sup> but also because of its low-cost availability and superior stability. Fc protein is highly productive in bacteria strains and is also quite thermostable in its deglycosylated form.<sup>54</sup> We have conducted a stability assessment, demonstrating that both SMDC and SMDC-Fc were quite stable at 37°C (Figure S14). We envisage that this SMDC-Fc scaffold, by being blessed with the cleavable Asn-linker, could be developed into a new molecular class for targeted cancer chemotherapy.

## MATERIALS AND METHODS

### Cell culture

KB, HeLa, NCI-N87, HepG2, and A549 cells were purchased from American Type Culture Collection. Upon thaw, HepG2 cells were

cultured in Roswell Park Memorial Institute 1640 medium (RPMI 1640, Gibco) supplemented with 10% fetal bovine serum (FBS; Gibco) and 1% penicillin-streptomycin (PS; Gibco). KB, HeLa, NCI-N87, and A549 cells were cultured in folate-free RPMI 1640 (Thermo Scientific) supplemented with 10% FBS and 1% PS. All cells were maintained in a humidified cell culture incubator at 37°C with 5% carbon dioxide (CO<sub>2</sub>).

### SMDC compounds

Synthesis details and characterization data of all SMDCs in this study are described in the [supplemental information](#).

### Protein expression, purification, and conjugation

Diglycyl Fc protein was prepared as we previously reported.<sup>10</sup> To achieve precise controlled and site-specific azido-labeling at the N terminus of the diglycyl Fc, a sortase A-mediated transpeptidation reaction was performed. Briefly, the purified diglycyl Fc protein (5 mg/mL) and pseudopeptide-656 (8 equivalent) were mixed in Tris-buffered saline, to which immobilized sortase A enzyme (1/400 equivalent) was added, and a transpeptidation reaction occurred. After 6 h of co-incubation at room temperature, the reaction was precipitated with 85% ammonium sulfate solution and further desalted with the G25 column aforementioned to yield the azido Fc protein. In order to visualize the azido Fc, sulfo-Cy3 DBCO can be added into the product before sample preparation of SDS-PAGE. All conjugation products were electrophoresed by SDS-PAGE to confirm their purity and MW. The final purified products (azido Fc) were concentrated by ultrafiltration and stored in PBS buffer containing 20% glycerol at –30°C.

### Fc grafting

SMDCs were conjugated with the azido Fc protein by CuAAC click reaction. Briefly, 5 mg/mL azido Fc protein was mixed with alkyne-functionalized SMDCs (4 equivalent) in PBS buffer containing 10% glycerol. The reaction was catalyzed by THPTA-stabilized Cu<sup>+</sup> and incubated at room temperature for 4 h. The reaction was precipitated with 85% ammonium sulfate solution and further desalted with the G25 column to yield the final products. All conjugates were analyzed by ESI-orthogonal acceleration (oa)-TOF MS to confirm the MW. The final products (SMDC-Fc) were concentrated by ultrafiltration (MW cutoff: 10 kDa) and stored in PBS buffer plus 20% glycerol at –30°C.

### LC-MS analysis

The normal LC-MS method for small molecules and SMDCs was performed as follows. Analytical characterization was performed using a Thermo Scientific Q Exactive Orbitrap LC-MS system. Typically, 5 µL injections were separated using a reversed-phase C18 column (3 × 50 mm, 3 µm, SHIMADZU). The eluent was monitored by UV (220, 254, and 280 nm) and MS (150–2,000 Da, ES+/ES–). The mobile-phase solvents were water with 0.1% formic acid (solvent A) and acetonitrile with 0.1% formic acid (solvent B). The flow rate was 0.3 mL/min with linear gradients from 95% A/5% B to 5% A/95% B over 10 min.

Analysis of SMDC-Fc was performed using a Waters SYNAPT G2-Si High-Definition MS system. Samples (~10  $\mu$ L of ~2 mg/mL stock) were separated using an ACQUITY UPLC Protein BEH C4 Column (300 Å, 1.7  $\mu$ m, 2.1  $\times$  50 mm, Waters Corporation) at 80°C by UV (280 nm) and MS (200–4,500 Da, ES<sup>-</sup>). The 5-min method used a flow rate of 0.2 mL/min with a gradient of buffer A (0.1% formic acid in water) and buffer B (0.1% formic acid in acetonitrile). The gradient running program is as follows: maintain 95% buffer A and 5% buffer B from 0 to 60 s, adjust to 5% buffer A and 95% buffer B as a gradient from 30 to 240 s, maintain 5% buffer A and 95% buffer B from 240 to 300 s. Samples (~20  $\mu$ L of ~1 mg/mL stock) were typically treated with 2  $\mu$ L 0.5 M TCEP immediately prior to analysis. SMDC-Fc were separated from reaction buffer salts using a Thermo Scientific Zeba Desalting Column before sampling. The raw charge envelope was deconvoluted using MassLynx software.

#### Cell binding and flow cytometry analysis

To assess the binding specificity to FR, all experiments were performed at room temperature to minimize the internalization upon receptor binding. Briefly, auristatin bioconjugates (sulfo-Cy5 labeled, Duoflour) were diluted within the different concentrations and co-incubated with cancer cells (~20,000 cells) for 2 h in serum-free RPMI 1640 media supplemented with 1% BSA. The cells were washed twice with PBS and analyzed on a BD LSR II flow cytometer (Beckton Dickinson).

#### IC<sub>50</sub> profiling

KB cells were seeded in a culture-treated 96-well clear plate (~3,000 cells per well) and allowed to grow for 24 h. The medium was replaced with a culture containing different concentrations of the test compounds (1:3 dilution steps) and incubated for 72 h. Cell viability was measured using the CCK-8 according to the protocol. Briefly, 15  $\mu$ L CCK-8 solution was added into the culture. After the 2-h incubation at 37°C, the absorbance at a wavelength of 450 nm was measured by a microplate reader (TECAN). IC<sub>50</sub> values were determined by fitting data to the three-parameter logistic equation, using Prism8 software (GraphPad Software) for data analysis.

#### Cathepsin B cleavage

Cathepsin B (bovine spleen) was purchased from Sigma-Aldrich. To activate the enzyme, it was incubated for 15 min with the buffer of 25 mM sodium acetate, 1 mM EDTA, and 10 mM DTT (pH 5.5) under ambient temperature. SMDCs (final concentration: 100  $\mu$ M) were mixed with 100 nM activated cathepsin B in the reaction buffer at 37°C. At indicated time points, 20  $\mu$ L of the solution was taken out, and each aliquot of the sample was immediately quenched by adding 10  $\mu$ L HPLC solvent (acetonitrile:water = 95:5 v/v, 0.1% formic acid). The samples were analyzed by HPLC using a gradient from 5% to 95% over 30 min. The hydrolysis fragments from the SMDC were identified through LC-MS analysis.

#### In vivo biodistribution

All the animal studies were performed in compliance with the guidelines of the Chinese Regulations for the Administration of Affairs

Concerning Experimental Animals and the Institutional Animal Care and Use Committee of Wuhan University. To minimize the impact of diet on serum folate levels, all mice (BALB/c nude) were fed a folic-acid-deficient diet 4 weeks ahead of tumor implantation and maintained throughout the experiments. KB cells ( $5 \times 10^6$ ) were then injected subcutaneously into the dorsal of 8-week-old BALB/c-nu mice. Tumor growth was measured 3 times per week, and size was calculated using the formula length  $\times$  width<sup>2</sup>/2. The bio-distribution study was performed when the KB tumor volume reached 400–600 mm<sup>3</sup>. Conjugates 2e-Fc (Cy7 labeled, 5 mg/kg) and 2e (Cy7 labeled, equal dye dose) were injected into mice via the tail vein in a volume of 200  $\mu$ L. Mice were then imaged using the IVIS *in vivo* imaging system (Bruker Xtreme BI) at 6, 24, 48, and 72 h. Food and water were provided normally during that period. At the end of the experiment, the mice were euthanized. The tumors and major organs (heart, lung, liver, spleen, and kidney) were harvested and imaged again for *ex vivo* analysis.

#### Pharmacokinetic studies

For pharmacokinetic studies, BALB/C mice were *i.v.* injected with either 2e (Cy7 labeled, 5 mg/kg) or 2e-Fc (sulfo-Cy7 labeled, equal dye dose) bioconjugates. Approximately 30  $\mu$ L blood was collected 0.25, 0.5, 1, 6, 24, 48, 72, 96, and 120 h after injection. Blood samples were imaged and quantified using an Odyssey CLx imaging system (LI-COR Biosciences).

#### Fluorescent histochemical analysis

C57BL/6 mice were injected *i.v.* with 5 mg/kg conjugates 2e-Fc (Cy5 labeled, 5 mg/kg) and 2e (Cy5 labeled, equal dye dose). Mice were sacrificed at the indicated time points, and organs were removed and fixed in 10% formalin (Sigma-Aldrich) overnight at 4°C. Fixed tissues were embedded in Tissue-Tek OCT Compound (Sakura), sliced into 10- $\mu$ m sections, mounted on pretreated glass slides, and mounted with Fluoroshield with DAPI histology mounting medium (Sigma-Aldrich). Sections were evaluated for the presence of conjugates using the Leica Aperio slide scanner.

#### In vivo therapy

KB xenografted tumors were implanted into BALB/c-nu mice as described above. When tumor sizes reached about 100 or 600 mm<sup>3</sup>, auristatin conjugates with Asn-linkers (2e or 2e-Fc) were administered as the dosage regimen recommended. Tumor growth and body weight were measured 3 times per week, and tumor size was calculated using methods as described above. The inoculated animals were examined daily to monitor the health condition. A ruffled coat, reluctance to move, sizable abdominal enlargement or ascites, or rapid weight loss was considered a sign of illness and toxicity. Animals were sacrificed when the termination criteria were reached.

#### Statistical analysis

All data are presented as mean  $\pm$  standard deviation. Independent-sample t tests were used to compare the means between two different groups. One-way analysis of variance was used to determine the

significance level with GraphPad Prism8 software, and  $p < 0.05$  were considered statistically significant.

## DATA AND CODE AVAILABILITY

All data presented in the main text or the [supplemental information](#) are available from the corresponding author upon request.

## SUPPLEMENTAL INFORMATION

Supplemental information can be found online at <https://doi.org/10.1016/j.ymthe.2024.02.020>.

## ACKNOWLEDGMENTS

This work was financially supported by the National Key R&D Program of China (grant no. 2021YFA0909900) and the National Natural Science Foundation of China (grant nos. 82073770 and 82273860).

## AUTHOR CONTRIBUTIONS

Conceptualization was performed by H.C. and W.T. Methodology was designed by Y.Z. and W.T. Investigation was performed by Y.Z. and R.X. Visualization was performed by H.C., and supervision was performed by W.T. The original manuscript was written by Y.Z. and was reviewed, commented on, edited, and approved by all authors.

## DECLARATION OF INTERESTS

Y.Z. and W.T. are listed as inventors on a patent application related to this work.

## REFERENCES

- Dumontet, C., Reichert, J.M., Senter, P.D., Lambert, J.M., and Beck, A. (2023). Antibody-drug conjugates come of age in oncology. *Nat. Rev. Drug Discov.* 22, 641–661. <https://doi.org/10.1038/s41573-023-00709-2>.
- Hurvitz, S.A. (2022). Recent progress in antibody-drug conjugate therapy for cancer. *Nat. Cancer* 3, 1412–1413. <https://doi.org/10.1038/s43018-022-00495-7>.
- Singh, D., Dheer, D., Samyutty, A., and Shankar, R. (2021). Antibody drug conjugates in gastrointestinal cancer: From lab to clinical development. *J. Control Release* 340, 1–34. <https://doi.org/10.1016/j.jconrel.2021.10.006>.
- Cazzamalli, S., Dal Corso, A., Widmayer, F., and Neri, D. (2018). Chemically Defined Antibody- and Small Molecule-Drug Conjugates for in Vivo Tumor Targeting Applications: A Comparative Analysis. *J. Am. Chem. Soc.* 140, 1617–1621. <https://doi.org/10.1021/jacs.7b13361>.
- Marks, I.S., Gardeen, S.S., Kurdziel, S.J., Nicolaou, S.T., Woods, J.E., Kularatne, S.A., and Low, P.S. (2018). Development of a Small Molecule Tubulysin B Conjugate for Treatment of Carbonic Anhydrase IX Receptor Expressing Cancers. *Mol. Pharm.* 15, 2289–2296. <https://doi.org/10.1021/acs.molpharmaceut.8b00139>.
- Krall, N., Pretto, F., Decurtins, W., Bernardes, G.J.L., Supuran, C.T., and Neri, D. (2014). A small-molecule drug conjugate for the treatment of carbonic anhydrase IX expressing tumors. *Angew. Chem. (International ed. English)* 53, 4231–4235. <https://doi.org/10.1002/anie.201310709>.
- Whalen, K.A., White, B.H., Quinn, J.M., Krikschiukaite, K., Alargova, R., Au Yeung, T.P., Bazinet, P., Brockman, A., DuPont, M.M., Oller, H., et al. (2019). Targeting the Somatostatin Receptor 2 with the Miniaturized Drug Conjugate, PEN-221: A Potent and Novel Therapeutic for the Treatment of Small Cell Lung Cancer. *Mol. Cancer Ther.* 18, 1926–1936. <https://doi.org/10.1158/1535-7163.mct-19-0022>.
- Kularatne, S.A., Wang, K., Santhapuram, H.K.R., and Low, P.S. (2009). Prostate-specific membrane antigen targeted imaging and therapy of prostate cancer using a PSMA inhibitor as a homing ligand. *Mol. Pharm.* 6, 780–789. <https://doi.org/10.1021/mp900069d>.
- Leamon, C.P., Vlahov, I.R., Reddy, J.A., Vetzal, M., Santhapuram, H.K.R., You, F., Bloomfield, A., Dorton, R., Nelson, M., Kleindl, P., et al. (2014). Folate-vinca alkaloid conjugates for cancer therapy: a structure-activity relationship. *Bioconjug. Chem.* 25, 560–568. <https://doi.org/10.1021/bc400441s>.
- Zheng, Y., Xu, R., Chen, S., and Tai, W. (2022). In vivo therapeutic effects of small molecule-drug conjugates enhanced by Fc grafting. *Biomaterials* 290, 121820. <https://doi.org/10.1016/j.biomaterials.2022.121820>.
- Lee, S.C., Ma, J.S.Y., Kim, M.S., Laborda, E., Choi, S.H., Hampton, E.N., Yun, H., Nunez, V., Muldong, M.T., Wu, C.N., et al. (2021). A PSMA-targeted bispecific antibody for prostate cancer driven by a small-molecule targeting ligand. *Sci. Adv.* 7, eabi8193. <https://doi.org/10.1126/sciadv.abi8193>.
- Gallo, F., Korsak, B., Müller, C., Hechler, T., Yanakieva, D., Avrutina, O., Kolmar, H., and Pahl, A. (2021). Enhancing the Pharmacokinetics and Antitumor Activity of an  $\alpha$ -Amanitin-Based Small-Molecule Drug Conjugate via Conjugation with an Fc Domain. *J. Med. Chem.* 64, 4117–4129. <https://doi.org/10.1021/acs.jmedchem.1c00003>.
- Vergote, I., and Leamon, C.P. (2015). Vintafolide: a novel targeted therapy for the treatment of folate receptor expressing tumors. *Ther. Adv. Med. Oncol.* 7, 206–218. <https://doi.org/10.1177/1758834015584763>.
- Oza, A., Vergote, I., Gilbert, L., Lucy, Ghatage, P., Lisyankaya, A., Ghamande, S., Chambers, S., Arranz, J., Provencher, D., et al. (2015). A randomized double-blind phase III trial comparing vintafolide (EC145) and pegylated liposomal doxorubicin (PLD/Doxil®/Caelyx®) in combination versus PLD in participants with platinum-resistant ovarian cancer (PROCEED) (NCT01170650). *Gynecol. Oncol.* 137, 5–6.
- Zhuang, C., Guan, X., Ma, H., Cong, H., Zhang, W., and Miao, Z. (2019). Small molecule-drug conjugates: A novel strategy for cancer-targeted treatment. *Eur. J. Med. Chem.* 163, 883–895. <https://doi.org/10.1016/j.ejmech.2018.12.035>.
- Peethambaram, P.P., Hartmann, L.C., Jonker, D.J., de Jonge, M., Plummer, E.R., Martin, L., Konner, J., Marshall, J., Goss, G.D., Teslenko, V., et al. (2015). A phase I pharmacokinetic and safety analysis of epothilone folate (BMS-753493), a folate receptor targeted chemotherapeutic agent in humans with advanced solid tumors. *Invest. New Drugs* 33, 321–331. <https://doi.org/10.1007/s10637-014-0171-9>.
- Falchook, G.S., Bendell, J.C., Ulahannan, S.V., Sen, S., Vilimas, R., Krikschiukaite, K., Mei, L., Jerkovic, G., Sarapa, N., Bilodeau, M., et al. (2020). Pen-866, a miniature drug conjugate of a heat shock protein 90 (HSP90) ligand linked to SN38 for patients with advanced solid malignancies: Phase I and expansion cohort results. *J. Clin. Oncol.* 38, 3515. [https://doi.org/10.1200/JCO.2020.38.15\\_suppl.3515](https://doi.org/10.1200/JCO.2020.38.15_suppl.3515).
- Johnson, M.L., Meyer, T., Halperin, D.M., Fojo, A.T., Cook, N., Blaszkowsky, L.S., Schlechter, B.L., Yao, J.C., Jemai, Y., Krikschiukaite, K., et al. (2018). First in human phase 1/2a study of PEN-221 somatostatin analog (SSA)-DM1 conjugate for patients (PTS) with advanced neuroendocrine tumor (NET) or small cell lung cancer (SCLC): Phase 1 results. *J. Clin. Oncol.* 36, 4097. [https://doi.org/10.1200/JCO.2018.36.15\\_suppl.4097](https://doi.org/10.1200/JCO.2018.36.15_suppl.4097).
- Salomon, P.L., Reid, E.E., Archer, K.E., Harris, L., Maloney, E.K., Wilhelm, A.J., Miller, M.L., Chari, R.V.J., Keating, T.A., and Singh, R. (2019). Optimizing Lysosomal Activation of Antibody-Drug Conjugates (ADCs) by Incorporation of Novel Cleavable Dipeptide Linkers. *Mol. Pharm.* 16, 4817–4825. <https://doi.org/10.1021/acs.molpharmaceut.9b00696>.
- Doronina, S.O., Mendelsohn, B.A., Bovee, T.D., Cervený, C.G., Alley, S.C., Meyer, D.L., Oflazoglu, E., Toki, B.E., Sanderson, R.J., Zabinski, R.F., et al. (2006). Enhanced activity of monomethylauristatin F through monoclonal antibody delivery: effects of linker technology on efficacy and toxicity. *Bioconjug. Chem.* 17, 114–124. <https://doi.org/10.1021/bc0502917>.
- Shen, B.Q., Xu, K., Liu, L., Raab, H., Bhakta, S., Kenrick, M., Parsons-Repointe, K.L., Tien, J., Yu, S.F., Mai, E., et al. (2012). Conjugation site modulates the in vivo stability and therapeutic activity of antibody-drug conjugates. *Nat. Biotechnol.* 30, 184–189. <https://doi.org/10.1038/nbt.2108>.
- Alley, S.C., Benjamin, D.R., Jeffrey, S.C., Okeley, N.M., Meyer, D.L., Sanderson, R.J., and Senter, P.D. (2008). Contribution of linker stability to the activities of anticancer immunoconjugates. *Bioconjug. Chem.* 19, 759–765. <https://doi.org/10.1021/bc7004329>.
- Fu, Z., Li, S., Han, S., Shi, C., and Zhang, Y. (2022). Antibody drug conjugate: the "biological missile" for targeted cancer therapy. *Signal Transduct. Target. Ther.* 7, 93. <https://doi.org/10.1038/s41392-022-00947-7>.

24. Caculitan, N.G., Dela Cruz Chuh, J., Ma, Y., Zhang, D., Kozak, K.R., Liu, Y., Pillow, T.H., Sadowsky, J., Cheung, T.K., Phung, Q., et al. (2017). Cathepsin B Is Dispensable for Cellular Processing of Cathepsin B-Cleavable Antibody-Drug Conjugates. *Cancer Res.* 77, 7027–7037. <https://doi.org/10.1158/0008-5472.can-17-2391>.
25. Li, F., Emmerton, K.K., Jonas, M., Zhang, X., Miyamoto, J.B., Setter, J.R., Nicholas, N.D., Okeley, N.M., Lyon, R.P., Benjamin, D.R., and Law, C.L. (2016). Intracellular Released Payload Influences Potency and Bystander-Killing Effects of Antibody-Drug Conjugates in Preclinical Models. *Cancer Res.* 76, 2710–2719. <https://doi.org/10.1158/0008-5472.can-15-1795>.
26. Bargh, J.D., Isidro-Llobet, A., Parker, J.S., and Spring, D.R. (2019). Cleavable linkers in antibody–drug conjugates. *Chem. Soc. Rev.* 48, 4361–4374. <https://doi.org/10.1039/C8CS00676H>.
27. Elgersma, R.C., Coumans, R.G.E., Huijbregts, T., Menge, W.M.P.B., Joosten, J.A.F., Spijker, H.J., de Groot, F.M.H., van der Lee, M.M.C., Ubink, R., van den Dobbelen, D.J., et al. (2015). Design, Synthesis, and Evaluation of Linker-Duocarmycin Payloads: Toward Selection of HER2-Targeting Antibody-Drug Conjugate SYD985. *Mol. Pharm.* 12, 1813–1835. <https://doi.org/10.1021/mp500781a>.
28. Poreba, M. (2020). Protease-activated prodrugs: strategies, challenges, and future directions. *FEBS J.* 287, 1936–1969. <https://doi.org/10.1111/febs.15227>.
29. Mondal, D., Ford, J., and Pinney, K.G. (2018). Improved Methodology for the Synthesis of a Cathepsin B Cleavable Dipeptide Linker, Widely Used in Antibody-Drug Conjugate Research. *Tetrahedron Lett.* 59, 3594–3599. <https://doi.org/10.1016/j.tetlet.2018.08.021>.
30. Dorywalska, M., Dushin, R., Moine, L., Farias, S.E., Zhou, D., Navaratnam, T., Lui, V., Hasa-Moreno, A., Casas, M.G., Tran, T.T., et al. (2016). Molecular Basis of Valine-Citrulline-PABC Linker Instability in Site-Specific ADCs and Its Mitigation by Linker Design. *Mol. Cancer Ther.* 15, 958–970. <https://doi.org/10.1158/1535-7163.mct-15-1004>.
31. Ubink, R., Dirksen, E.H.C., Rouwette, M., Bos, E.S., Janssen, I., Egging, D.F., Loosveld, E.M., van Achterberg, T.A., Berentsen, K., van der Lee, M.M.C., et al. (2018). Unraveling the Interaction between Carboxylesterase 1c and the Antibody-Drug Conjugate SYD985: Improved Translational PK/PD by Using Ces1c Knockout Mice. *Mol. Cancer Ther.* 17, 2389–2398. <https://doi.org/10.1158/1535-7163.mct-18-0329>.
32. Zhao, H., Gulesserian, S., Malinao, M.C., Ganesan, S.K., Song, J., Chang, M.S., Williams, M.M., Zeng, Z., Mattie, M., Mendelsohn, B.A., et al. (2017). A Potential Mechanism for ADC-Induced Neutropenia: Role of Neutrophils in Their Own Demise. *Mol. Cancer Ther.* 16, 1866–1876. <https://doi.org/10.1158/1535-7163.mct-17-0133>.
33. Anami, Y., Yamazaki, C.M., Xiong, W., Gui, X., Zhang, N., An, Z., and Tsuchikama, K. (2018). Glutamic acid–valine–citrulline linkers ensure stability and efficacy of antibody–drug conjugates in mice. *Nat. Commun.* 9, 2512. <https://doi.org/10.1038/s41467-018-04982-3>.
34. Chuprakov, S., Ogunkoya, A.O., Barfield, R.M., Bauzon, M., Hickie, C., Kim, Y.C., Yeo, D., Zhang, F., Rabuka, D., and Drake, P.M. (2021). Tandem-Cleavage Linkers Improve the In Vivo Stability and Tolerability of Antibody-Drug Conjugates. *Bioconjug. Chem.* 32, 746–754. <https://doi.org/10.1021/acs.bioconjchem.1c00029>.
35. Miller, J.T., Vitro, C.N., Fang, S., Benjamin, S.R., and Tumej, L.N. (2021). Enzyme-Agnostic Lysosomal Screen Identifies New Legumain-Cleavable ADC Linkers. *Bioconjug. Chem.* 32, 842–858. <https://doi.org/10.1021/acs.bioconjchem.1c00124>.
36. Choe, Y., Leonetti, F., Greenbaum, D.C., Lecaillon, F., Bogoy, M., Brömme, D., Ellman, J.A., and Craik, C.S. (2006). Substrate profiling of cysteine proteases using a combinatorial peptide library identifies functionally unique specificities. *J. Biol. Chem.* 281, 12824–12832. <https://doi.org/10.1074/jbc.M513331200>.
37. Trindade, A.F., Frade, R.F.M., Maçôas, E.M.S., Graça, C., Rodrigues, C.A.B., Martinho, J.M.G., and Afonso, C.A.M. (2014). Click and go: simple and fast folic acid conjugation. *Org. Biomol. Chem.* 12, 3181–3190. <https://doi.org/10.1039/c4ob00150h>.
38. Figliola, C., Marchal, E., Groves, B.R., and Thompson, A. (2019). A step-wise synthetic approach is necessary to access  $\gamma$ -conjugates of folate: folate-conjugated prodiosenes. *RSC Adv.* 9, 14078–14092. <https://doi.org/10.1039/c9ra01435g>.
39. Hong, V., Presolski, S.I., Ma, C., and Finn, M.G. (2009). Analysis and optimization of copper-catalyzed azide-alkyne cycloaddition for bioconjugation. *Angew. Chem. (International ed. English)* 48, 9879–9883. <https://doi.org/10.1002/anie.200905087>.
40. Pyzik, M., Kozicky, L.K., Gandhi, A.K., and Blumberg, R.S. (2023). The therapeutic age of the neonatal Fc receptor. *Nat. Rev. Immunol.* 23, 415–432. <https://doi.org/10.1038/s41577-022-00821-1>.
41. D’Hooghe, L., Chalmers, A.D., Heywood, S., and Whitley, P. (2017). Cell surface dynamics and cellular distribution of endogenous FcRn. *PLoS one* 12, e0182695. <https://doi.org/10.1371/journal.pone.0182695>.
42. Widdison, W.C., Ponte, J.F., Coccia, J.A., Lanieri, L., Setiady, Y., Dong, L., Skaletskaya, A., Hong, E.E., Wu, R., Qiu, Q., et al. (2015). Development of Anilino-Maytansinoid ADCs that Efficiently Release Cytotoxic Metabolites in Cancer Cells and Induce High Levels of Bystander Killing. *Bioconjug. Chem.* 26, 2261–2278. <https://doi.org/10.1021/acs.bioconjchem.5b00430>.
43. Dubowchik, G.M., Firestone, R.A., Padilla, L., Willner, D., Hofstead, S.J., Mosure, K., Knipe, J.O., Lasch, S.J., and Trail, P.A. (2002). Cathepsin B-labile dipeptide linkers for lysosomal release of doxorubicin from internalizing immunoconjugates: model studies of enzymatic drug release and antigen-specific in vitro anticancer activity. *Bioconjug. Chem.* 13, 855–869. <https://doi.org/10.1021/bc025536j>.
44. Gräwe, A., and Stein, V. (2021). Linker Engineering in the Context of Synthetic Protein Switches and Sensors. *Trends Biotechnol.* 39, 731–744. <https://doi.org/10.1016/j.tibtech.2020.11.007>.
45. Markowska, A., Markowski, A.R., and Jarocka-Karpowicz, I. (2021). The Importance of 6-Aminohexanoic Acid as a Hydrophobic, Flexible Structural Element. *Int. J. Mol. Sci.* 22, 12122. <https://doi.org/10.3390/ijms222212122>.
46. Cheng, X., Li, J., Tanaka, K., Majumder, U., Milinichik, A.Z., Verdi, A.C., Maddage, C.J., Rybinski, K.A., Fernando, S., Fernando, D., et al. (2018). MORAb-202, an Antibody-Drug Conjugate Utilizing Humanized Anti-human FR $\alpha$  Farletuzumab and the Microtubule-targeting Agent Eribulin, has Potent Antitumor Activity. *Mol. Cancer Ther.* 17, 2665–2675. <https://doi.org/10.1158/1535-7163.mct-17-1215>.
47. Erickson, H.K., Park, P.U., Widdison, W.C., Kovtun, Y.V., Garrett, L.M., Hoffman, K., Lutz, R.J., Goldmacher, V.S., and Blättler, W.A. (2006). Antibody-maytansinoid conjugates are activated in targeted cancer cells by lysosomal degradation and linker-dependent intracellular processing. *Cancer Res.* 66, 4426–4433. <https://doi.org/10.1158/0008-5472.can-05-4489>.
48. Liu, Y., Zhou, F., Sang, H., Ye, H., Chen, Q., Yao, L., Ni, P., Wang, G., and Zhang, J. (2017). LC–MS/MS method for the simultaneous determination of Lys-MCC-DM1, MCC-DM1 and DM1 as potential intracellular catabolites of the antibody–drug conjugate trastuzumab emtansine (T-DM1). *J. Pharm. Biomed. Anal.* 137, 170–177. <https://doi.org/10.1016/j.jpba.2017.01.011>.
49. Leal, M., Wentland, J., Han, X., Zhang, Y., Rago, B., Duriga, N., Spriggs, F., Kadar, E., Song, W., McNally, J., et al. (2015). Preclinical Development of an anti-5T4 Antibody-Drug Conjugate: Pharmacokinetics in Mice, Rats, and NHP and Tumor/Tissue Distribution in Mice. *Bioconjug. Chem.* 26, 2223–2232. <https://doi.org/10.1021/acs.bioconjchem.5b00205>.
50. Du, B., Yu, M., and Zheng, J. (2018). Transport and interactions of nanoparticles in the kidneys. *Nat. Rev. Mater.* 3, 358–374. <https://doi.org/10.1038/s41578-018-0038-3>.
51. Pyzik, M., Rath, T., Kuo, T.T., Win, S., Baker, K., Hubbard, J.J., Grenha, R., Gandhi, A., Krämer, T.D., Mezo, A.R., et al. (2017). Hepatic FcRn regulates albumin homeostasis and susceptibility to liver injury. *Proc. Natl. Acad. Sci. USA* 114, E2862–E2871. <https://doi.org/10.1073/pnas.1618291114>.
52. Mackness, B.C., Jaworski, J.A., Boudanova, E., Park, A., Valente, D., Mauriac, C., Pasquier, O., Schmidt, T., Kabiri, M., Kandira, A., et al. (2019). Antibody Fc engineering for enhanced neonatal Fc receptor binding and prolonged circulation half-life. *mAbs* 11, 1276–1288. <https://doi.org/10.1080/19420862.2019.1633883>.
53. Lee, C.H., Kang, T.H., Godon, O., Watanabe, M., Delidakis, G., Gillis, C.M., Sterlin, D., Hardy, D., Cogné, M., Macdonald, L.E., et al. (2019). An engineered human Fc domain that behaves like a pH-toggle switch for ultra-long circulation persistence. *Nat. Commun.* 10, 5031. <https://doi.org/10.1038/s41467-019-13108-2>.
54. Qin, K., Shi, W., Zhao, L., Li, M., Tang, Y., Faridoun, Jiang, B., Jiang, B., Tang, F., and Huang, W. (2020). Thermostability detection and optimization of glycoengineered antibodies and antibody–drug conjugates based on differential scanning calorimetry analysis. *Bioorg. Chem.* 94, 103391. <https://doi.org/10.1016/j.bioorg.2019.103391>.